Journal of Geophysical Research, 119(4), 3584-3600

AGU PUBLICATIONS

JGR

Journal of Geophysical Research: Solid Earth

RESEARCH ARTICLE

10.1002/2013JB010901

Key Points:
- An updated kinematic model for the East African Rift
- Geodetic data consistent with three subplates
- Outward displacement corrections along SWIR need revision

Supporting Information:
- Readme
- Table S1
- Table S2

Correspondence to:
E. Calais,
eric.calais@ens.fr

Citation:
Saria, E., E. Calais, D. S. Stamps, D. Delvaux, and C. J. H. Hartnady (2014), Present-day kinematics of the East African Rift, *J. Geophys. Res. Solid Earth*, *119*, doi:10.1002/2013JB010901.

Received 4 DEC 2013
Accepted 12 MAR 2014
Accepted article online 20 MAR 2014

Present-day kinematics of the East African Rift

E. Saria[1], E. Calais[2], D. S. Stamps[3,4], D. Delvaux[5], and C. J. H. Hartnady[6]

[1]Department of Geomatics, School of Geospatial Sciences and Technology, Ardhi University, Dar Es Salaam, Tanzania, [2]Department of Geosciences, UMR CNRS 8538, Ecole Normale Supérieure, Paris, France, [3]Department of Earth and Atmospheric Sciences, Purdue University, West Lafayette, Indiana, USA, [4]Now at Department of Earth, Atmospheric, and Planetary Sciences, Massachusetts Institute of Technology, Cambridge, Massachusetts, USA, [5]Royal Museum for Central Africa, Tervuren, Belgium, [6]Umvoto Africa (Pty) Ltd, Cape Town, South Africa

Abstract The East African Rift (EAR) is a type locale for investigating the processes that drive continental rifting and breakup. The current kinematics of this ~5000 km long divergent plate boundary between the Nubia and Somalia plates is starting to be unraveled thanks to a recent augmentation of space geodetic data in Africa. Here we use a new data set combining episodic GPS measurements with continuous measurements on the Nubian, Somalian, and Antarctic plates, together with earthquake slip vector directions and geologic indicators along the Southwest Indian Ridge to update the present-day kinematics of the EAR. We use geological and seismological data to determine the main rift faults and solve for rigid block rotations while accounting for elastic strain accumulation on locked active faults. We find that the data are best fit with a model that includes three microplates embedded within the EAR, between Nubia and Somalia (Victoria, Rovuma, and Lwandle), consistent with previous findings but with slower extension rates. We find that earthquake slip vectors provide information that is consistent with the GPS velocities and helps to significantly reduce uncertainties of plate angular velocity estimates. We also find that 3.16 Myr MORVEL average spreading rates along the Southwest Indian Ridge are systematically faster than prediction from GPS data alone. This likely indicates that outward displacement along the SWIR is larger than the default value used in the MORVEL plate motion model.

1. Introduction

The East African Rift (EAR), the ~5000 km long divergent boundary between the Nubian and Somalian plates (Figure 1), is a type locale for rifting and continental breakup [e.g., *Wilson*, 1966]. A detailed understanding of the distribution of present-day strain across and along the EAR is essential to provide quantitative constraints to mechanical models of the rifting process. Early estimates of the current Nubia-Somalia plate motion were based on oceanic data in the Red Sea [*Jestin et al.*, 1994] or along the Southwest Indian Ridge [*Chu and Gordon*, 1999]. These 3.2 Myr average geological estimates have since been refined [*Horner-Johnson et al.*, 2005, 2007; *DeMets et al.*, 2010] and are now complemented by present-day estimates derived from space geodetic data. The first Nubia-Somalia angular velocities derived from geodetic data relied solely on three GPS sites (SEY1, REUN, and MALI) on the Somalian plate and showed significant scatter [*Sella et al.*, 2002; *Kreemer et al.*, 2003; *Prawirodirdjo and Bock*, 2004; *Nocquet et al.*, 2006]. Follow-up studies included additional kinematic data such as earthquake slip vector directions [*Calais et al.*, 2006] and spreading rates and transform fault azimuths along the South West Indian Ridge (SWIR) [*Stamps et al.*, 2008]. More recent studies using longer time series and additional sites on the Somalian plate are now providing Nubia-Somalia angular velocities that agree with each other within errors, as well as with geological estimates [e.g., *Argus et al.*, 2010; *Altamimi et al.*, 2012; *Saria et al.*, 2013].

The EAR is composed of a series of fault-bounded basins and volcanic centers stretching through East Africa in a roughly NS direction, with seismicity, active faulting, and volcanism generally localized along narrow belts separating largely aseismic domains. This led *Hartnady* [2002] to postulate the existence of microplates (among which the Victoria, Rovuma, and Lwandle microplates discussed in this paper, Figure 1) embedded between the main Nubia and Somalia plates. *Calais et al.* [2006] tested this hypothesis using a sparse geodetic data set augmented by earthquake slip vector directions along the main branches of the EAR and estimated the angular velocity of the Victoria microplate. *Stamps et al.* [2008] improved these results using an augmented geodetic data set, earthquake slip vector directions along the EAR, and the transform fault directions and 3.16 Myr average spreading rates along the SWIR published by

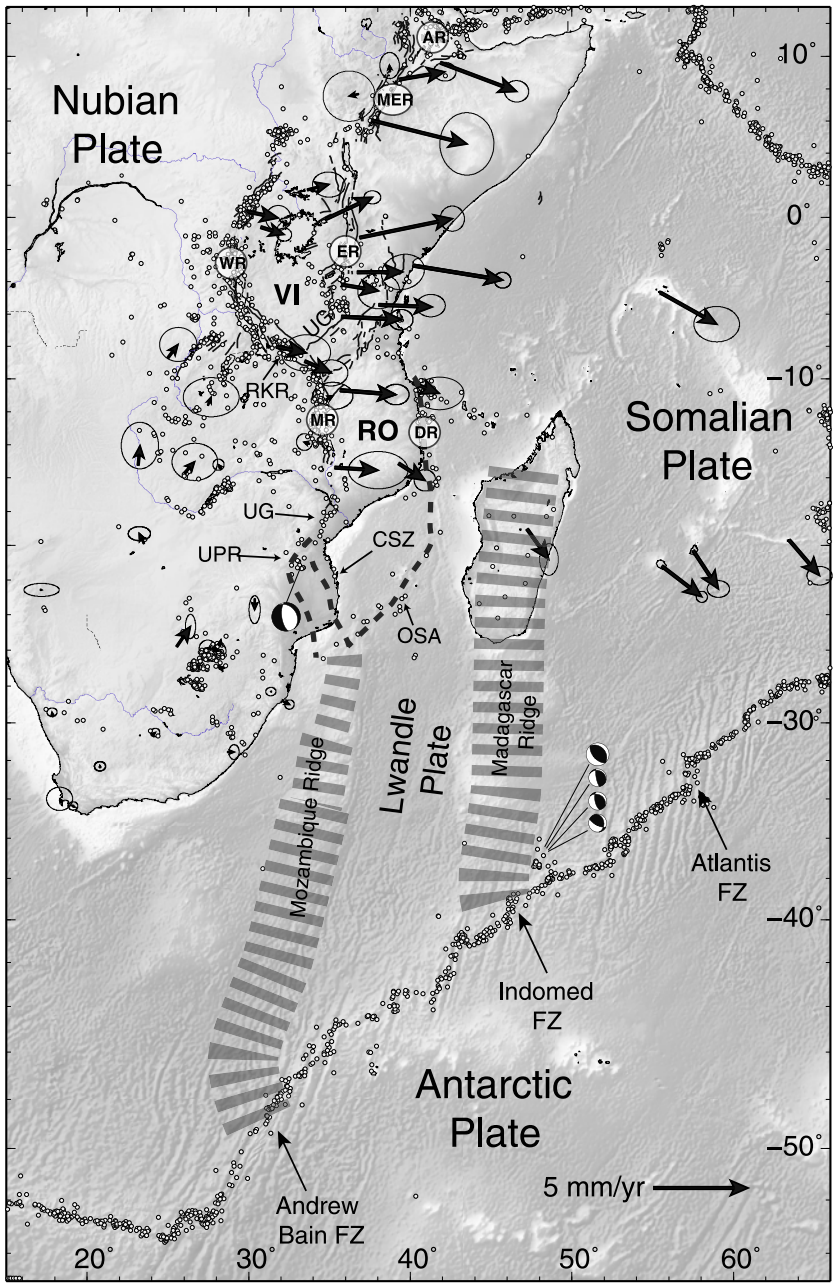

Figure 1. Present-day tectonic setting of the East African Rift. Solid black lines show major active faults [from *Skobelev et al.*, 2004], small back circles show seismicity (National Earthquake Information Center (NEIC) catalog), dashed lines indicate inferred plate boundary traces, and hatched areas over Madagascar and the Madagascar Ridge show the possibly diffuse Lwandle-Somalia plate boundary. Black arrows show a selection of the GPS data set used here, with 95% confidence ellipses. The focal mechanism of the *M*7.5, 22 February 2006, Mozambique earthquake is shown [*Fenton and Bommer*, 2006], as well as the focal mechanisms of a cluster of thrust events at the southern end of the Madagascar Ridge (NEIC). MER = Main Ethiopian Rift, WR = Western Rift, ER = Eastern Rift, MR = Malawi Rift, DR = Davie Ridge, CSZ = Chissenga seismic zone, UG = Urema graben, UPR = Urrongas protorift, USA = Quathlamba Seismic Axis, RK = Rukwa, and UG = Usangu basin.

Horner-Johnson et al. [2007]. However, their angular velocity estimates for Rovuma and Lwandle were poorly constrained, as they included only one geodetic datum on each plate. More recently, thanks to a rapid increase of continuous geodetic sites in Africa, *Saria et al.* [2013] calculated a plate motion model for the Nubia-Somalia-Victoria-Rovuma plate system from geodetic data alone. *Déprez et al.* [2013], with a smaller GPS data set, obtained similar results within uncertainties. However, neither model included the Lwandle

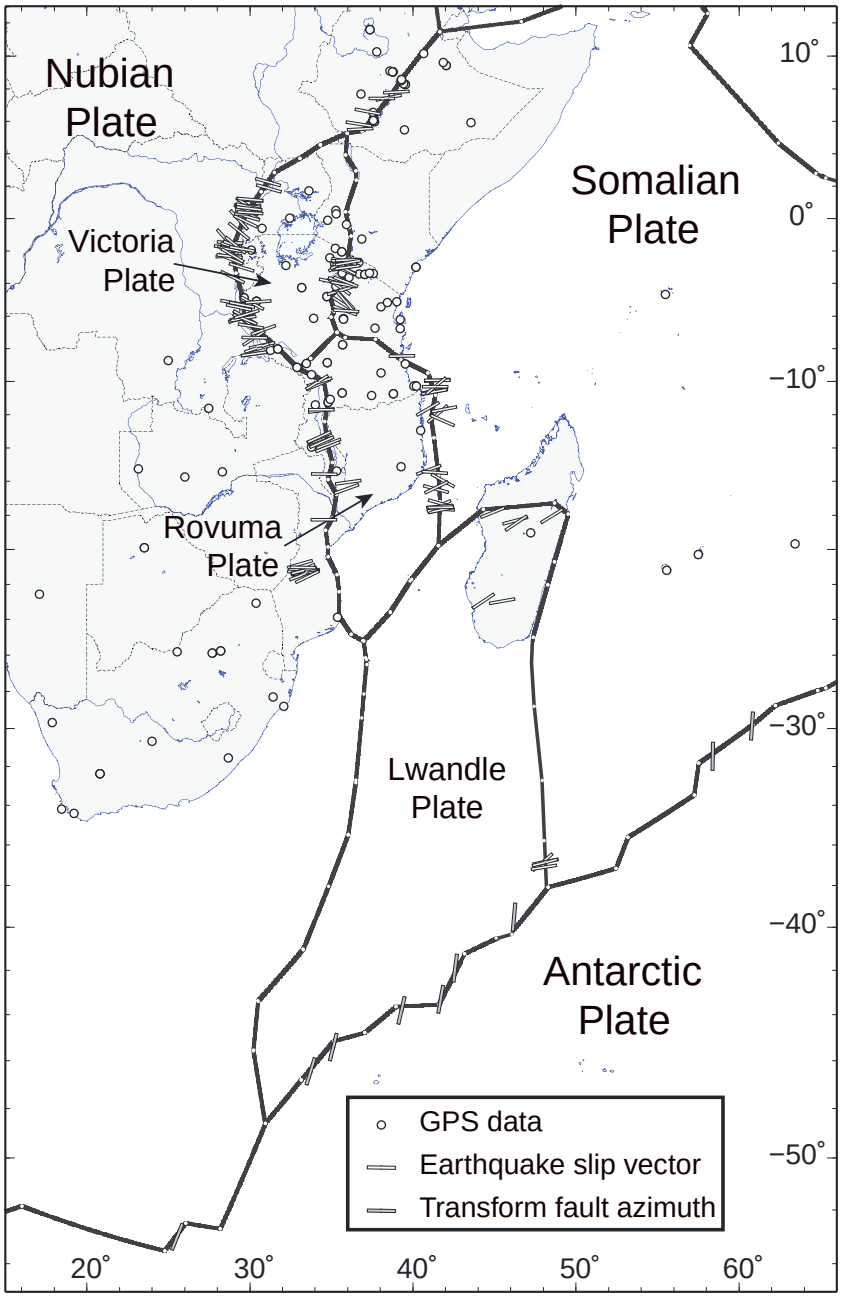

Figure 2. Spatial distribution of the GPS, earthquake slip vector, and transform fault azimuth data used in this paper. Solid black lines show the block boundaries used in the kinematic model (explanations in the text).

microplate as it is mostly oceanic and contains only one GPS site in Madagascar. Also, the kinematic models proposed so far do not use recent acquisitions of episodic GPS data in East Africa.

Here we revisit the kinematics of the EAR using significantly augmented data sets (Figure 2), including newly available episodic GPS data from Ethiopia and Tanzania, an improved earthquake slip vector database [*Delvaux and Barth*, 2009], the new MORVEL spreading rate and transform azimuth data set on the SWIR [*DeMets et al.*, 2010], and an improved geodetic definition of stable Nubia [*Saria et al.*, 2013]. The additional GPS data now available in the EAR are such that many sites are located close enough to active faults that they are likely experiencing elastic strain accumulation (assuming that the faults are locked to typical mid-crustal depths, as shown by hypocenter distribution in the EAR [*Craig et al.*, 2011]). Therefore, this work uses

a model that solves for rigid plate rotations while allowing elastic strain accumulation on plate-bounding faults [*McCaffrey*, 2002]. Finally, we pay particular attention to the constraints provided by the 3.16 Myr average geologic data along the SWIR and its agreement with GPS-only plate motion estimates.

2. Regional Setting

The EAR stretches through East Africa quasi-continuously from the Afar depression in northern Ethiopia to the Southwest Indian Ridge (SWIR) at the junction with the Antarctic plate (Figure 1). It encompasses the youngest continental flood basalt province (Ethiopia) and is superimposed on a broad region of high topographic elevation (~1000 m high eastern and southern African plateaus). This high elevation region and its offshore extension in the southeastern Atlantic define the "African Superswell" [*Nyblade and Robinson*, 1994], which lies on average 500 m higher than the global topographic mean. The analysis of long-wavelength gravity and topographic relief over Africa shows that more than half of this anomalous topography is dynamically supported [*Lithgow-Bertelloni and Silveri*, 1998; *Gurnis et al.*, 2000] by convective mantle upwelling associated with a large, slow shear wave seismic velocity mantle anomaly, the African superplume [*Ritsema et al.*, 1998]. The initiation of Cenozoic rifting is estimated to start in the mid-Tertiary with the onset of volcanism in the Turkana Rift [*Furman et al.*, 2006] followed by uplift and flood basalts in Ethiopia [*Pik et al.*, 2003]. The process was followed by extension in the Main Ethiopian Rift and the western and eastern (Kenya) branches [*Roberts et al.*, 2012], and further south in the Malawi Rift [*Lyons et al.*, 2011]. We describe hereafter the main active tectonic features of the EAR, which we use to delineate the geometry of the block model described below.

The northernmost branch of the EAR is the Main Ethiopian Rift, a single-extensional rift basin between Nubia and Somalia extending from the Afar triple junction [*Wolfenden et al.*, 2004; *Keir et al.*, 2009] to the Lake Turkana depression in northern Kenya. South of Lake Turkana, seismic and tectonic activity delineate two branches, the Eastern and Western Rifts, which bound a relatively unfaulted, aseismic domain centered on a 2.5–3 Ga old assemblage of metamorphic and granitic terranes (Tanzanian craton) that has remained undisturbed tectonically since the Archean [e.g., *Chesley et al.*, 1999], except for minor seismicity under Lake Victoria. This domain was interpreted by *Hartnady* [2002] as the present-day Victoria microplate. Seismic, xenolith and gravity data show that the 150–200 km thick lithosphere of the Tanzanian craton is colder and stronger than surrounding orogenic belts [*Wendlandt and Morgan*, 1982; *Boyd and Gurney*, 1986; *Green et al.*, 1991; *Ritsema et al.*, 1998; *Weeraratne et al.*, 2003].

Most of the seismicity of the EAR is concentrated in the magma-poor Western Rift, which initiated around 25 Ma simultaneously with the Eastern branch [*Roberts et al.*, 2012]. The Western branch is characterized by low-volume volcanic activity, large ($M > 6.5$) magnitude earthquakes, and hypocenters at depths up to 30–40 km [*Yang and Chen*, 2010; *Craig et al.*, 2011]. From Lake Albert to southern Rukwa, the width of the Western branch does not extend more than 40–70 km, with large volcanic centers coincident with the basin segmentation (Virunga, South-Kivu, and Rungwe). The Western Rift connects southward with the Malawi Rift via the reactivated Mesozoic Rukwa Rift [*Delvaux et al.*, 2012]. The Malawi Rift itself shares similarities with the Tanganyika basin, with long and well-defined normal faults (e.g., Livingstone escarpment) and limited volcanism. The 2009 Karonga earthquake swarm, with 4 $Mw > 5.5$ events [*Biggs et al.*, 2010], however, showed that additional hanging wall normal faults participate in present-day extension. Recent coring in Lake Malawi indicates that modern rift initiation may be as young as early to middle Pliocene, considerably younger than most prior estimates [*Lyons et al.*, 2011].

In contrast, the Eastern branch is characterized by a broad zone of shallow (5–15 km) and smaller magnitude seismicity, but voluminous volcanism [e.g., *Dawson*, 1992; *Yang and Chen*, 2010; *Craig et al.*, 2011]. The Eastern Rift includes the ~25 Ma Turkana Rift, which reactivates part of an Eocene-Oligocene rift system [*George et al.*, 1998; *Pik et al.*, 2006]. South of Lake Turkana, rifting and volcanism initiated at about 25 Ma [*Furman et al.*, 2006; *McDougall and Brown*, 2009] with active eruptive centers along its length and moderate seismic activity. The seismically active southernmost part of the Eastern Rift, < 5 Myr old in the Natron basin, experienced in 2007 a discrete strain accommodation event rarely observed in a continental rift, with slow slip on a normal fault followed by a dike intrusion [*Calais et al.*, 2008; *Biggs et al.*, 2009].

South of the Natron basin, the Eastern branch of the EAR splits into the Pangani, Manyara, and Eyasi Rifts at an apparent triple junction (North Tanzanian Divergence, NTD) [*Le Gall et al.*, 2004, 2008]. The continuation of the Eastern branch south of the NTD appears more prominent along the Manyara Rift [*Macheyeki et al.*,

2008], which may therefore form the eastern boundary of the Victoria plate. The aseismic plateau between the Manyara and Pangani Rifts has been interpreted as a microplate (Masai block), separate from Victoria and Somalia [*Dawson*, 1992; *Le Gall et al.*, 2008].

Farther south, the Manyara and Pangani Rifts connect with the Usangu basin to the southwest and with the Kerimbas Rift to the east. The presence of 17–19 Ma phonolites intruding the basin sediments [*Rasskazov et al.*, 2003] indicates that the Usangu basin likely initiated in the early stage of rift development. The Usangu basin shows moderate seismicity and connects to the south with the Malawi Rift, while the Kerimbas Rift is continuous offshore with the Davie Ridge, a narrow, NS trending, zone of seismicity with purely east-west extensional focal mechanisms [*Mougenot et al.*, 1986; *Grimison and Chen*, 1988]. The southward continuation of the Davie Ridge is unclear, but it may connect with the Quathlamba Seismic Axis, a linear cluster of seismicity between Madagascar and southern Mozambique [*Hartnady*, 1990; *Hartnady et al.*, 1992]. South of the Malawi Rift, active deformation extends along the seismically active Urema graben and further south along the Chissenga seismic zone and the Urrongas protorift swell [*Hartnady*, 2006], where the *Mw*7.0 Machaze, Mozambique, earthquake of 23 February 2006 occurred [*Fenton and Bommer*, 2006; *Yang and Chen*, 2008].

South of the hypothetic junction between the Chissenga and Quathlamba seismic zones, little data are available on active deformation or seismicity, making the location of the Lwandle-Nubia plate boundary uncertain. *Hartnady* [1990], on the basis of several moderate to strong earthquakes in 1941, 1942, 1956, 1969, 1972, 1975, 1981, and 1989, proposed a boundary that cuts across eastern South Africa and continues southward through the old oceanic crust of the submarine Natal Valley and Transkei basin. However, the most recent analyses of GPS data from the dense South Africa TRIGNET array do not detect relative motion at a significant level between eastern South Africa and Nubia [*Saria et al.*, 2013; *Malservisi et al.*, 2013]. The Lwandle-Nubia plate boundary is, however, well defined at the SWIR, where *Horner-Johnson et al.* [2007] show that it coincides with the Andrew Bain Fracture Zone (Figure 1). In the absence of more definite data on the location of that boundary, we chose the simplest solution and hypothesize that the Lwandle-Nubia plate boundary connects the Chissenga-Quathlamba junction with the Andrew Bain Fracture Zone along the prominent bathymetric scarp that marks the eastern edge of the Mozambique Ridge. Alternate hypothesis are possible, including a boundary encompassing the location of a zone of faulting across the deep abyssal plain of the submarine Natal Valley [*Reznikov et al.*, 2005] and the m_b 5.9, 7 April 1975 event in the Transkei basin (latitude = −37.6237, longitude = 30.9846; International Seismological Centre Online Bulletin, http://www.isc.ac.uk). However, the exact location of that plate boundary has no effect on the model results described hereafter because we do not use GPS or earthquake slip vector data in that region.

3. Input Data

The input data used in this study (Figure 2) include both present-day information on active deformation from 164 GPS velocities and 167 earthquake slip vector directions, and 3.16 Ma average transform fault directions and spreading rates along the SWIR [*DeMets et al.*, 2010]. Compared to *Stamps et al.* [2008], the GPS data used here are a six-fold increase in number and now cover all major tectonic blocks, while earthquake slip vector directions are 3 times more numerous.

3.1. GPS Velocities

The GPS velocities used here result from the processing of 17 years of continuous and episodic data in Africa and its close surroundings. Continuous data include sites operated in the framework of the International Global Navigation Satellite Systems (GNSS) Services (IGS), sites installed and operated by various research groups in Africa, and sites installed and operated by national agencies. It is necessary that data from additional continuous GPS stations be made openly available in the near future to strengthen the definition of the Africa Reference Frame (AFREF) [*Wonnacott*, 2005, 2006; *Saria et al.*, 2013]. Episodic GPS data come mostly from Tanzania and span 2005–2011. They serve to better determine the kinematics of the central part of the EAR, in particular the motion of the Victoria and Rovuma microplates.

We processed the GPS data using the GAMIT-GLOBK software [*Herring et al.*, 2010]. We first use, for each day, the doubly differenced GPS phase observations to estimate daily station coordinates, satellite state vectors, seven tropospheric delay parameters at each station per day, two horizontal tropospheric gradients per day, and phase ambiguities. We use the IGS final orbits and Earth Orientation Parameters [*International Earth Rotation Service*, 2003], apply an absolute antenna phase center correction using the latest International

Terrestrial Reference Frame 2008 (ITRF2008)-compatible IGS table [*Schmid et al.*, 2007], and apply corrections for solid Earth tides, polar tides, and ocean loading using the International Earth Rotation Service standards [*McCarthy and Petit*, 2003].

The loosely constrained daily solution vectors and their variance-covariance matrix for station and orbital elements (= quasi-observations) are then combined with global Solution Independent Exchange (SINEX) files from the IGS daily processing routinely done at the Massachusetts Institute of Technology (MIT) in order to integrate our regional solution in a global frame. We finally implement the International Terrestrial Reference Frame by minimizing position and velocity deviations at 191 globally distributed stations well defined in ITRF2008 [*Altamimi et al.*, 2011]. We use the daily solution to produce coordinate time series, which we use to identify and correct for discontinuities and outliers, as well as to estimate time-correlated noise based on extrapolating to infinite time a first-order Gauss-Markov fit to the observation time series in order to obtain realistic velocity uncertainties [*Reilinger et al.*, 2006]. We implement this information into weekly (loose) combinations of the daily quasi-observations in order to reduce daily scatter and processing time. We finally combine the loose weekly solutions into a cumulative position/velocity solution expressed in ITRF2008 (Table S1 in the supporting information).

In order to better define the Somalia-Nubia relative motion along the Main Ethiopian Rift we also use the GPS solution from *Kogan et al.* [2012] but removed sites whose velocities were poorly determined (sites DBMK, ARMI, DANA, BDAR, DAMY, GOD2, GEWA, KOGA, SNBT, SULA, CNTO, SERO, PDSO, DOBI, OVLK, SMRA, TNDH, KSGT, MEBK, KOGA, KOLO, ADIS, and ADD1) because of short data time span or monument instability. We transformed the remaining velocity into the reference frame defined above by estimating and applying a seven parameter transformation using sites common to both solutions. Residual velocities at sites common to both solutions are 1.2 mm/yr and 0.9 mm/yr on average for the north and east components, respectively (Table S2). The largest residual is at site ARMI, for which our solution differs significantly from that of *Kogan et al.* [2012].

Finally, we include GPS velocities at 19 additional sites on the Antarctic plate (C. DeMets, personal communication, 2013) that were not in our solution in order to better determine the motion of that plate. As for the Ethiopia data set mentioned above, we transformed these velocities into the reference frame used here by estimating and applying a seven parameter transformation using sites common to both solutions. We find that the kinematic modeling results are similar to the ones obtained without this extra data set but that the uncertainty on the Antarctic plate angular velocity decreases significantly. Residual velocities at sites common to both solutions are 0.2 mm/yr and 0.1 mm/yr on average for the north and east components, respectively (maximum 0.3 mm/yr; Table S2).

3.2. Earthquake Slip Vectors

We include in our solution 167 earthquake slip vector directions calculated from first motion analysis and body-waveform inversion. Seventy percent of them come from the global centroid moment tensor (CMT) project [*Ekstrom et al.*, 2012], and the remaining 30% come from regional studies, all listed in *Delvaux and Barth* [2009] and in *Yang and Chen* [2010]. For each event, we chose the focal solution provided in the most recent regional study, then relied on the CMT solution if no regional solution was available. The catalog we use covers the 1976–2011 time period. We assigned each earthquake slip vector to one of the microplate boundaries that define our model geometry (Main Ethiopian Rift, Western Rift, Eastern Rift, Malawi Rift, Madagascar and southern end of the Madagascar Ridge, Davie Ridge).

Most earthquakes in the EAR have extensional focal mechanisms, with a few exceptions such as strike-slip events at the southern end of the western branch (not used in our model), and a cluster of reverse faulting events at the southern end of the Madagascar Ridge with slip directions oriented ~45°N (Figure 1). As noted by *Horner-Johnson et al.* [2007], these latter events, together with extensional events well documented in Madagascar, imply a counterclockwise rotation of the Lwandle plate with respect to Somalia.

Slip vector directions exhibit some scatter but are generally consistent along each rift segment, with some systematic variability, as seen for instance along the Tanganyika segment of the Western Rift (Figure 2). There, slip vector directions rotate progressively from north to south from ~NW-SE, to E-W, then SW-NE, a pattern consistent with the rotation of the Victoria microplate.

The uncertainty associated with earthquake slip vector directions is usually not quoted in the corresponding publications. We therefore chose to assign a uniform uncertainty to all slip vector directions, which we

determined by computing their scatter within clusters of nearby slip vectors. We found a value of 20° which we further scaled in the block model inversion so that the reduced χ^2 for the entire slip vector data set is close to unity. We find a scaling factor of 0.8, indicating that actual uncertainty on earthquake slip vector directions may be on the order of 15–20°.

3.3. SWIR Transform Fault and Spreading Rate Data

The SWIR is an ultraslow spreading ridge which has only been investigated directly since the 1990s. The 3.16 Ma (anomaly 2A) average transform fault direction and spreading rate data along the SWIR led *Lemaux et al.* [2002] then *Horner-Johnson et al.* [2005] to show that relative plate motions across the southwestern and northeastern parts of the SWIR were significantly different, indicative of the differential motion of Nubia and Somalia with respect to Antarctica. *Horner-Johnson et al.* [2007] further showed that the Somalia-Antarctica-Nubia-Arabia plate circuit closure could be significantly improved by assigning the central portion of the SWIR to the Lwandle plate proposed by *Hartnady* [2002]. *DeMets et al.* [2010] confirmed, through a global plate circuit, that the eastern, middle, and western thirds of the SWIR are indeed recording the motion of three different plates (Nubia, Lwandle, and Somalia) with respect to Antarctica.

Here we follow the segmentation proposed in MORVEL [*DeMets et al.*, 2010] (Figure 1) and assign SWIR transform directions and spreading rates (1) west of the Andrew Bain Fracture Zone (~30°E) to Nubia-Antarctica, (2) from the Andrew Bain to the Indomed Fracture Zone (~50°E) to Lwandle-Antarctica, and (3) east of the Atlantis II Fracture Zone (~60°E) to Somalia-Antarctica. We do not use data between the Indomed and Atlantis II Fracture Zones, which bound the probably diffuse—and poorly defined—boundary between the Somalia and Lwandle plates [*Horner-Johnson et al.*, 2007].

We therefore used a total of 12 transform fault directions and 104 spreading rates and their associated uncertainties along the three segments of the SWIR defined above. For both data types, we used the uncertainties provided in the MORVEL data set without alteration. We note here that the MORVEL spreading rates are all adjusted downward to account for a 2 km outward displacement correction [*Atwater and Mudie*, 1973] along the SWIR, as for all other spreading ridges except for the Reykjanes (5 km) and Carlsberg Ridges (3.5 km) [details in *DeMets et al.*, 2010].

4. Methodology

4.1. Defining a Nubia-Fixed Frame

The significant increase of continuous GPS stations in Africa in the recent years provides a much improved data set to define a Nubia-fixed frame over the one used by *Stamps et al.* [2008]. Active deformation within Nubia is attested by volcanism along the Cameroon Volcanic Line [e.g., *Moreau et al.*, 1987; *Ubangoh et al.*, 1997] as well as seismic activity marking the propagation of rifting into Zambia, Zimbabwe, Congo, and Botswana (Luangwa, Mweru, and Upemba grabens) [e.g., *Tedesco et al.*, 2007; *Njome et al.*, 2010]. This deformation is, however, limited in magnitude as shown by recent analyses based on continuous space geodetic sites in Africa indicating at most 0.6 mm/yr of internal deformation within Nubia [*Saria et al.*, 2013; *Déprez et al.*, 2013; *Malservisi et al.*, 2013].

Because the GPS solution used here is slightly different from the one of *Saria et al.* [2013], we determined a new set of sites for the definition of stable Nubia. We select sites with at least 2.5 years of observation and velocity uncertainties lower than 1.5 mm/yr. We compute the Nubia angular velocity using all the sites that fulfill these criteria then remove one site at a time and test its consistency with the rigid plate motion defined by the remaining set of sites using an *F* ratio test. This procedure leads to 28 sites that fit Nubia rigid plate motion with a reduced χ^2 of 1.3 and a weighted root-mean-square residual (WRMS) of 0.5 mm/yr (sites TAMP, SUTH, SUTM, NKLG, WIND, ZAMB, GOUG, ETJI, PRE1, PRE2, DIFA, OUAG, DJOU, BJCO, BJAB, BJSA, MSKU, INHB, TDOU, HNUS, ULDI, GAO1, SHEB, ULUB, NIAM, RUST, BKGP, and UNEC).

4.2. Block Model

We model GPS velocities as the sum of (1) the rigid rotation of the (micro)plate on which the site resides, and (2) the contribution of strain accumulation on all (micro)plate-bounding faults. This simple kinematic model is implemented in the DEFNODE program [*McCaffrey*, 2002] which we use for this study. Earthquake slip vectors and transform fault azimuths are modeled as the direction of relative motion between the two plates on either side of the block boundary to which the data belong. Similarly, oceanic spreading rates are modeled as the velocity of the relative motion between the two plates on either side of the block boundary

Table 1. Best Fit Model Statistics: Number of Observations Used (#Obs), χ^2, Reduced χ^2 (i.e., χ^2 Divided by Degree of Freedom N), and Weighted Root-Mean-Square (WRMS)

	#Obs	χ^2	χ^2/N	WRMS
All[a]	497	5.620E+02	1.17	—
Slip[a]	167	6.510E+03	1.09	4.10
GPS[a]	330	7.080E+04	1.14	0.43
Nubia[b]	128	2.161E+01	0.73	0.31
Victoria[b]	54	2.160E+02	1.31	0.78
Somalia[b]	64	9.520E+02	1.15	0.66
Rovuma[b]	32	1.030E+02	0.89	0.64
Antarctica[b]	50	6.060E+04	1.76	0.35
Lwandle[b]	2	8.050E+00	0.50	0.34

[a]Statistics by data type.
[b]Statistics by plate.

to which the data belong. The strain accumulation component at GPS sites is calculated using a back slip approach [*Savage*, 1983] and the Green's functions from dislocation theory in an elastic half space [*Okada*, 1992]. We assume that faults are fully locked in the seismogenic upper crust to a given depth. In this configuration, we solve for the (micro)plate angular velocities (with respect to Nubia), which one can then use to calculate relative motions along boundary faults.

Our block model geometry consists of three major plates—Nubia, Somalia, and Antarctica—plus three smaller ones—Victoria, Rovuma, and Lwandle—whose boundaries follow the major rift structures described above (Figure 2). South of the Malawi Rift, and in the absence of new information, we follow the block geometry of *Stamps et al.* [2008]. We assume that the broad deformation zone encompassing the Madagascar Ridge and the island of Madagascar marks the Lwandle-Somalia boundary [*Kusky et al.*, 2007]. No earthquakes or geological observations are available along the poorly defined Victoria-Rovuma and Rovuma-Lwandle boundaries. We tentatively draw the former along a belt of moderate seismicity and recent faulting in the Usangu-Ruaha-Kilombero grabens [*Le Gall et al.*, 2004], and the latter along the Quathlamba Seismic Axis [*Hartnady*, 1990]. Block boundary contours serve to assign GPS velocities to the appropriate plate. Their exact location only impacts the model results if GPS sites are located close enough to them to be affected by the elastic strain accumulation signal they may cause.

Fault locking depth and dip angles are not well known in the EAR. We therefore assign constant values for all faults in the model. We recognize that they are likely to vary amongst rift-bounding faults (in particular as a function of the regional thermomechanical regime), but we currently lack sufficient information to implement these variations in the model. We could have equated locking depth with maximum earthquake depth—as is often assumed for strike-slip faults in a thermally stable crust. However, this is questionable in the EAR given the variety of earthquake hypocenter depths [e.g., *Albaric et al.*, 2009] and the existence of deep events [*Yang and Chen*, 2010; *Craig et al.*, 2011] in a crust whose thermal structure varies strongly laterally. We therefore ran a series of models with fault locking depth varying between 5 and 55 km and fault dip angle between 45° and 90° and scored the models according to their fit to the data. We find the minimum model χ^2 for locking depth of 20 km and a fault dip of 75°.

5. Results and Discussion

5.1. Best Fit Model

Our best fit model uses 164 GPS velocities, 167 earthquake slip vectors, 104 spreading rates, and 12 transform fault azimuths (Figure 2) and has an overall reduced χ^2 of 1.2 (Table 1). Reduced χ^2 values for individual data sets and for each plate angular velocity estimate are also close to unity. WRMS is 0.4 mm/yr for GPS velocities and 4° for earthquake slip vector directions. Data, model, and residuals GPS velocities for the central part of the EAR, where our GPS data set is the most dense, can be inspected graphically on Figure 3. The fit between observations and model predictions is usually good, with, however, significant residuals around the southern part of Eastern Rift in Tanzania. The data at our disposal are not sufficient to determine whether this represents a true tectonic and/or magmatic signal or is simply data noise. The fit between observed and modeled earthquake slip vector directions is good as well (Figure 4), with model predictions within the data uncertainty for 72% of the observations. The model, however, misses some of the systematic variability in earthquake slip vector directions along the Tanganyika segment of the Western Rift. In particular, we suspect that the misfit at the southern termination of the Tanganyika Rift reflects the motion of an independent Rukwa block, as proposed by *Delvaux et al.* [2012]. The data at our disposal are not sufficient to test this hypothesis, which would require additional GPS measurements in this region.

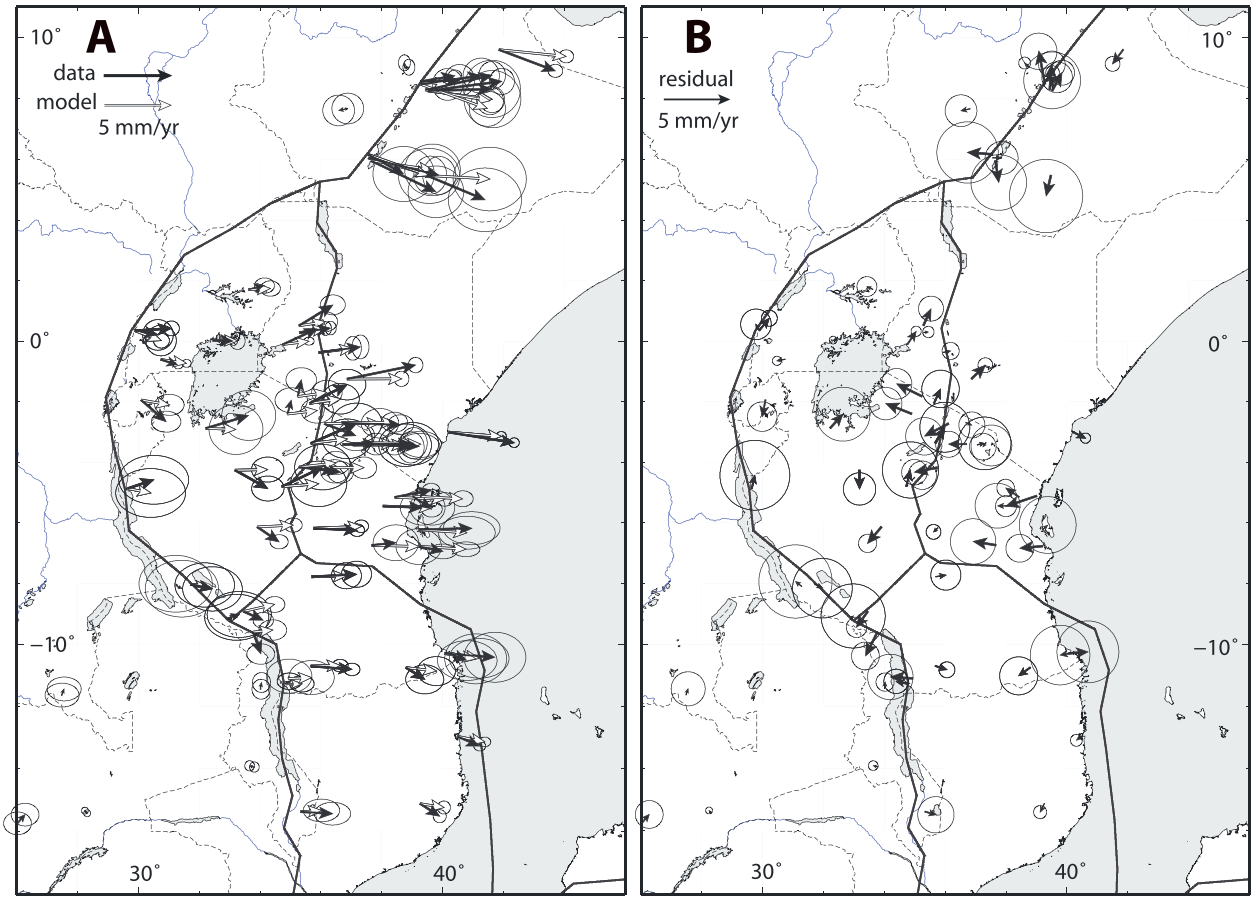

Figure 3. (a) GPS observations and kinematic block model predictions in the central part of the East African Rift. (b) Residual velocities (model minus observation). Error ellipses are 95% confidence.

While testing for the compatibility between the various data sets, we found that the GPS data for Nubia-Antarctica were not consistent with the MORVEL spreading rates along the SWIR. This is illustrated in Figure 5, which shows that an inversion where GPS sites in Antarctica are unweighted results in a 1–2 mm/yr systematic overprediction of their velocities, while SWIR spreading rates are well predicted. Reciprocally, a solution where SWIR spreading rates are unweighted provides an excellent fit to the GPS velocities on Antarctica but systematically underpredicts SWIR spreading rates by ~2 mm/yr. This could result from a recent acceleration in plate motions across the SWIR or could alternatively be an artifact of the outward displacement correction applied in MORVEL.

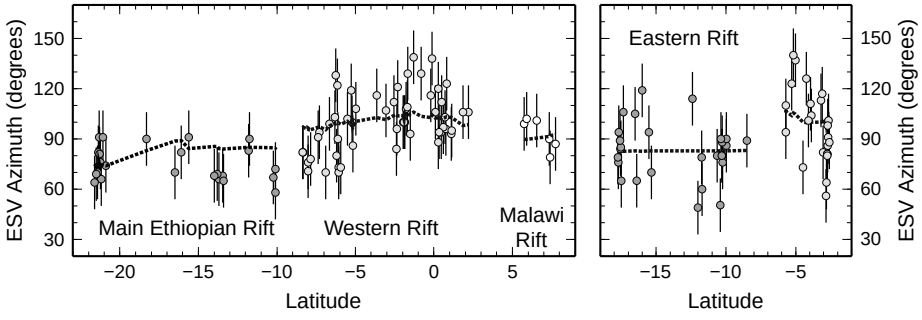

Figure 4. Comparison between observed earthquake slip vector directions (circles) and prediction of the best fit model along the different segments of the East African Rift. Error bars are 95% confidence.

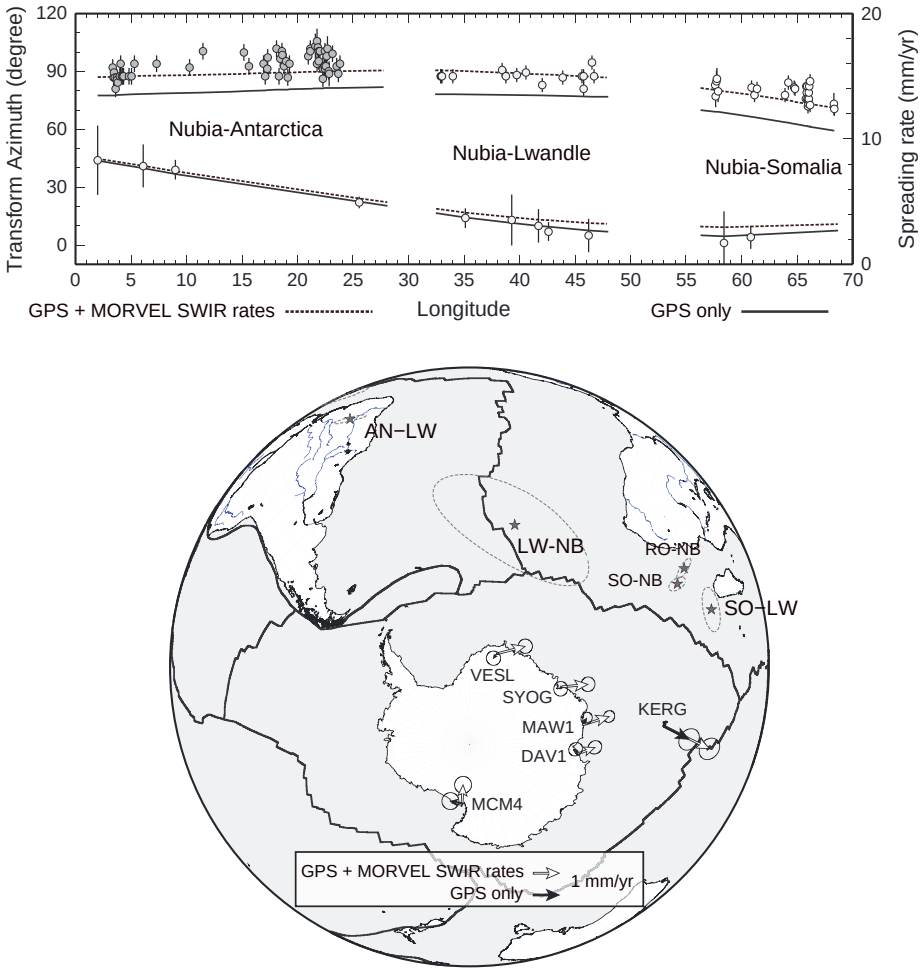

Figure 5. Comparison between a model that uses SWIR spreading rates, GPS velocities, and earthquake slip vector directions along the EAR and a model that uses GPS velocities and earthquake slip vector directions only. (top) Observed (circles) and predicted (lines) SWIR spreading rates and transform fault azimuths. Note the ~1–2 mm/yr systematic misfit when SWIR spreading rates are included. (bottom) Residual (observed-model) velocities on the Antarctic plate. Note the systematic ~2 mm/yr residuals when SWIR spreading rates are included. Error ellipses are 95% confidence.

As quoted in *DeMets et al.* [2010], the 2 km outward correction applied in MORVEL at most ridges (except the Reykjanes Ridge—5.0 km—and the Carlsberg Ridge—3.5 km) reduces spreading rates by 0.63 mm/yr (when calculated since anomaly 2A). Increasing the outward displacement correction along the SWIR to 5 km would decrease spreading rate along the SWIR by 1.6 mm/yr, making it consistent with the prediction of our GPS-only (or GPS + earthquake slip vectors) model. A recent study of the Nubia-Antarctica plate motion for the past 20 Ma shows a very steady spreading rate along the SWIR for the past 8 Ma (C. DeMets, personal communication, 2013), consistent with present rates if a 5 km outward displacement correction is applied, and in excellent agreement with the prediction from our GPS-only model. Finally, we note that transform fault azimuths along the SWIR are perfectly consistent with predictions from our GPS-only model and hence provide no indication of a recent plate motion change. Given the inconsistency between the SWIR spreading rates from the MORVEL data set and the GPS velocities on Antarctica and given the possibility that the outward displacement correction applied to SWIR spreading rates in MORVEL underestimates the actual value, we therefore decided not to use SWIR spreading rates in our preferred model.

Table 3 and Figure 6 display the angular velocities describing the rotation of the Somalia, Victoria, Rovuma, and Lwandle plates with respect to Nubia. Our estimate of the Somalia angular rotation is consistent with the most recent estimates based on GPS data alone [*Argus et al.*, 2010; *Altamimi et al.*, 2012; *Saria et al.*, 2013] (Figure 7). It is also consistent, within uncertainties, with the estimates from *Horner-Johnson et al.* [2007] and *DeMets et al.* [2010], both based on geologic data alone. The only notable difference between

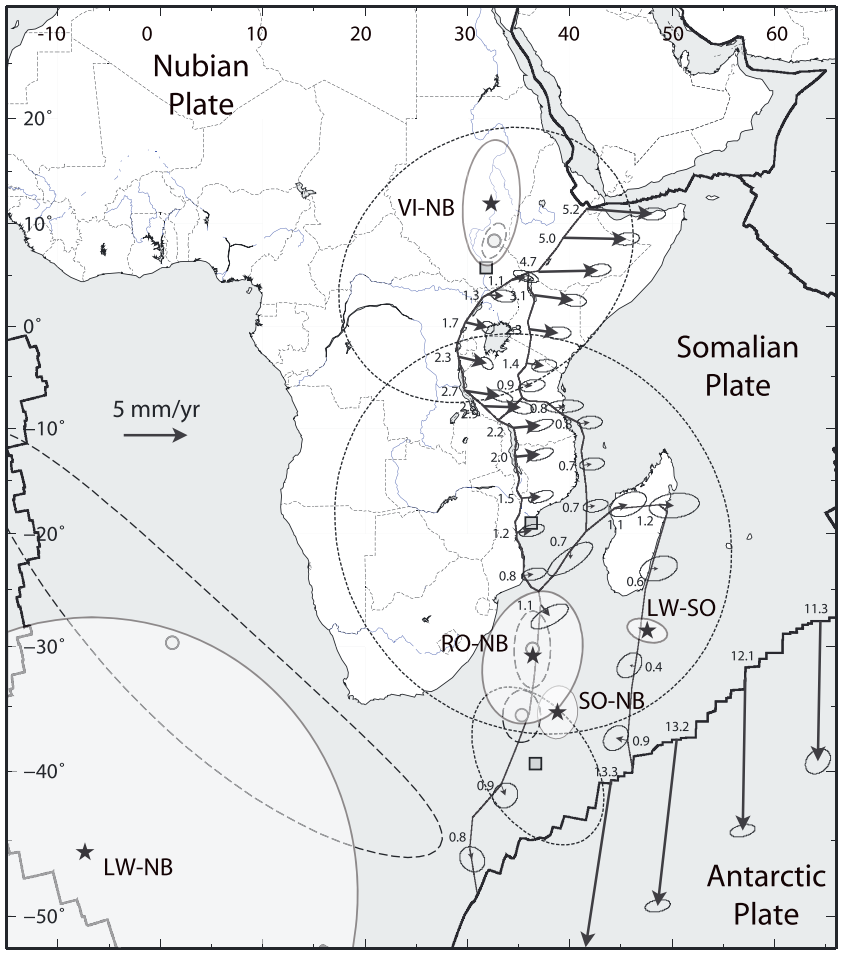

Figure 6. Best fit model. Black arrows show predicted relative motions between adjacent blocks; numbers are velocities in mm/yr. Error ellipses are 95% confidence. Circles: Euler poles from *Stamps et al.* [2008]. Squares: Euler poles from *Saria et al.* [2013]. Stars: Euler poles from this study. Euler poles are shown with their 95% confidence limit.

our Nubia-Somalia angular velocity and the recent estimates mentioned above is a slower rotation rate, as also found by *Saria et al.* [2013] who used a GPS solution similar to the one used here. These slower rates remain, however, consistent with previous estimates at the 95% confidence level, except with that of *Stamps et al.* [2008] (Figure 7, left). The Victoria Euler pole (Figure 6) implies a counterclockwise rotation of that microplate, as found by several recent studies [e.g., *Stamps et al.*, 2008; *Saria et al.*, 2013; *Déprez et al.*, 2013] and is consistent with these previous estimates. The Rovuma Euler pole plots very close to that of *Stamps et al.* [2008] in spite of a GPS data set that is significantly augmented. Its location, south of the microplate, is consistent with the extension observed along the Urongas protorift and the Chissenga seismic zone (including the 2006, *M*7.5 purely extensional earthquake in southern Mozambique (Figure 1)). The Lwandle angular velocity remains poorly determined but is consistent, within uncertainties, with that of *Stamps et al.* [2008].

5.2. Tests

Given the small relative motions predicted by our model for the Rovuma-Somalia and Lwandle-Somalia plate boundaries and given the relative proximity of the Victoria-Nubia and Rovuma-Nubia Euler poles, we tested whether the data were fit significantly better with a five-plate model compared to models with fewer plates. To do so, we determined whether the decrease in χ^2 of a model with fewer plates compared to a more complex one was significant using the *F* ratio statistics [e.g., *Stein and Gordon*, 1984], given by

$$F = \frac{(\chi^2_{p_1} - \chi^2_{p_2})/(p_1 - p_2)}{\chi^2_{p_2}/p_2} \quad (1)$$

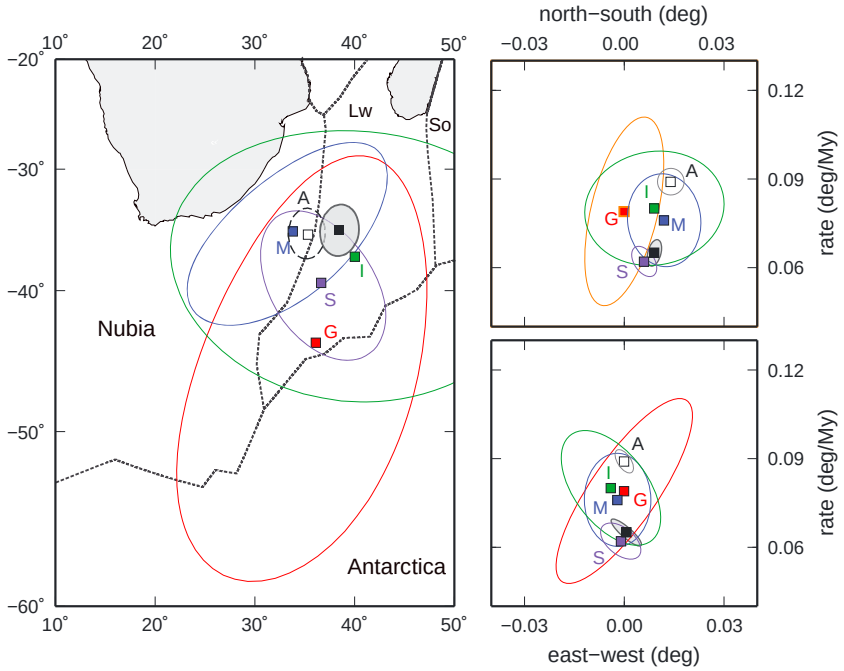

Figure 7. Angular velocities for Nubia-Somalia and 95% confidence limits in three perpendicular planes. (left) Rotation poles, (right, bottom) profile from west to east, and (right, top) profile from south to north. Our best estimate (black square) is compared to recent solutions by *Stamps et al.* [2008] (A), *Argus et al.* [2010] (G), *DeMets et al.* [2010] (M), *Altamimi et al.* [2012] (I), and *Saria et al.* [2013] (S).

where $\chi^2_{p_1}$ and $\chi^2_{p_2}$ are the chi-square statistics of two models with p_1 and p_2 degrees of freedom, respectively. We compare this experimental F ratio to the expected value of a $F(p_1 - p_2, p_1)$ distribution for a given risk level α% (or a $100 - \alpha$% confidence level) that the null hypothesis (the decrease in χ^2 is not significant) can be rejected. Results (Table 2) compare a case where Victoria, Rovuma, and Lwandle are part of Somalia (null hypothesis), with three case where the Victoria, Rovuma, then Lwandle plates are successively separated from Somalia. We find that the null hypothesis can be rejected with high confidence level (> 99%) for these three cases. We also compare a case where Victoria, Rovuma, and Lwandle form a single plate independent from Somalia (null hypothesis), with a case where the Victoria, Rovuma, then Lwandle plates are split off. Again, we find that the null hypothesis can be rejected with high confidence level (> 99%) for these three new cases. We therefore conclude that the new data used here, which include significantly more GPS velocities compared to previous models, justify dividing the EAR into three subplates.

We also compared the best fit angular velocities presented above with estimates derived from GPS velocities only (Table 3). Results are similar to the best fit model but with significantly larger uncertainties. This comparison can be further quantified by determining whether the decrease in χ^2 from a model with GPS plus earthquake slip vector data to a model with GPS velocities only is significant, using the F ratio test described above. We find that the probability that the decrease in χ^2 is significant is only 24%, indicating that the GPS-only model is not significantly better than the joint GPS + earthquake

Table 2. Statistical Tests For Independent Microplates in the EAR[a]

		F Ratio (Experimental)	*F* ratio (Expected)		
Plate Geometry	# of Data	*F*	95% Conf.	99% Conf.	Result
Nubia, (Somalia + Victoria + Rovuma + Lwandle)	-	-	-	-	Null Hypothesis
Nubia, Victoria, (Somalia + Rovuma + Lwandle)	484	31	2.63	3.83	$F > f$
Nubia, Victoria, Rovuma, (Somalia + Lwandle)	503	14	2.12	2.85	$F > f$
Nubia, Somalia, Victoria, Rovuma, and Lwandle	514	12	1.90	2.45	$F > f$
Nubia, Somalia, (Victoria + Rovuma + Lwandle)	514	0.19	2.62	3.82	$F < f$

[a]Names between parentheses indicate blocks bounded together into a single plate in the tests.

Table 3. Angular Velocity Estimates From This Study

	Degrees		(deg/Myr)		Error Ellipse (deg)			Ang. Rot. (10^{-5} rad/Myr)			Covariance (10^{-10} rad^2/Myr^2)					
Plate	Lat	Lon	ω	σ_ω	S_{maj}	S_{min}	azim	Ω_X	Ω_Y	Ω_Z	c_{xx}	c_{xy}	c_{xz}	c_{yy}	c_{yz}	c_{zz}
Entire Data Set																
Somalia	34.44	−142.19	0.065	0.002	4.3	3.2	7.6	−73.92	−57.36	64.16	13	15	−2	11	−1	4
Victoria	12.14	32.54	0.076	0.012	12.4	5.5	4.4	109.32	69.75	27.90	247	305	−2	96	−2	5
Rovuma	30.68	−143.46	0.057	0.004	11.2	8.0	18.6	−68.74	−50.94	50.76	86	60	−10	46	−15	22
Lwandle	45.28	172.87	0.016	0.004	36.9	35.9	29.0	−19.51	2.44	19.84	39	18	−0	54	−15	64
Antarctica	−3.69	139.36	0.128	0.001	1.4	0.5	90.0	−169.17	145.21	−14.38	1	1	−0	1	−2	5
GPS Only																
Somalia	37.47	−143.54	0.060	0.004	5.1	2.3	162.7	−66.85	−49.39	63.71	26	23	−5	26	−6	5
Victoria	15.44	31.77	0.062	0.026	17.9	2.7	174.8	88.68	54.92	28.81	1620	1058	−35	697	−23	6
Rovuma	27.74	−147.00	0.066	0.030	18.7	3.4	165.0	−85.51	−55.53	53.62	1808	1370	−492	1050	−375	146
Lwandle	35.97	175.96	0.022	0.008	43.9	14.3	59.5	−30.00	2.19	22.55	146	14	−76	105	−74	99
Antarctica	−4.91	139.31	0.129	0.001	2.7	0.8	19.8	−170.09	146.25	−19.27	3	1	−4	3	−4	17

[a]Lat and lon are the latitude and longitude of the Euler pole, S_{maj}, S_{min}, and azim are the semimajor axis, semiminor axis, and azimuth (clockwise from north) of the corresponding error ellipse (95% confidence). The angular rotation rate is ω, and σ_ω is its uncertainty. Ω_X, Ω_Y, and Ω_Z are the three Cartesian coordinates of the angular rotation vector in units of 10^{-5} rad/Myr. The upper triangular elements of the corresponding variance-covariance matrix in units of 10^{-10} rad^2/Myr^2 are c_{xx}, c_{xy}, c_{xz}, c_{yy}, c_{yz}, and c_{zz}.

slip vector best fit model. We conclude that the earthquake slip vector data set used here is consistent with the GPS velocities, which justifies using them jointly to determine the present-day kinematics of the EAR. Including earthquake slip vectors in kinematic models for the EAR is particularly important for plates that are poorly covered by GPS data, such as Rovuma and Lwandle.

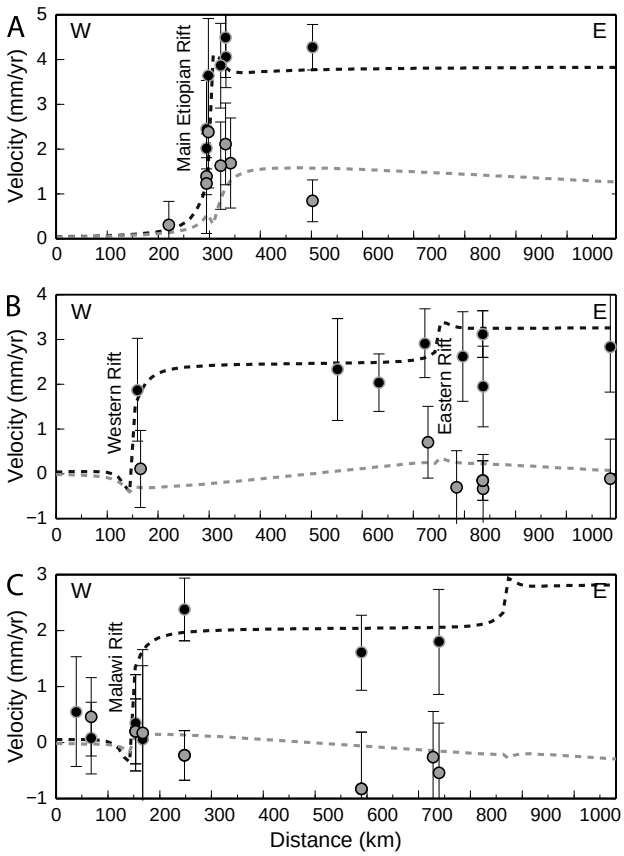

Figure 8. Rift-perpendicular velocity profiles across three selected locations showing the best fit elastic dislocation model (dashed lines, black = rift perpendicular, grey = rift parallel) and GPS observations (circles). (a) Main Ethiopian Rift, (b) Western and Eastern Rifts, and (c) Malawi rift.

5.3. Predicted Extension Rates Along the EAR

Our best fit model predicts extension rates across the EAR basins up to 5.2 ± 0.9 mm/yr (95% confidence) at the Afar triple junction. This is consistent with the 5.4 mm/yr prediction of *Saria et al.* [2013], who use a similar GPS data set, but somewhat slower than previous models (7.0 mm/yr [*Stamps et al.*, 2008], 6.2 mm/yr [*DeMets et al.*, 2010], and 7.2 mm/yr [*Argus et al.*, 2010] for the most recent ones). Model extension rates decrease southward overall, reaching less than 1 mm/yr in the southern most part of the EAR. The extension rates found here are generally slower than those of *Stamps et al.* [2008]. For instance, we find 2.8 mm/yr of extension at the southern tip of the Tanganyika Rift, where *Stamps et al.* [2008] calculated 4.1 mm/yr. The same holds for the Malawi Rift, where our models show 1.5–2.2 mm/yr whereas *Stamps et al.* [2008] predicted 2.7–2.8 mm/yr. Conversely, our model predicts slightly faster rates across the Davie Ridge (up to 1 mm/yr). Motion between the Lwandle plate and its surrounding Nubian and Somalian are predicted to

occur at very slow rates (<1 mm/yr), except in Madagascar with 1.5 mm/yr of east-west extension, consistent with the very small amount of seismic moment release in these regions in the historical catalog.

We also observe that the central and northern parts of the EAR (north of about 25°S) show purely east-west directed extension, regardless of the trend of the rift basins. This implies that a small component of left-lateral strike-slip motion may occur in the northern segments of the Western branch (Albertine basin) and a small component of right-lateral strike-slip motion may occur in the southernmost part of the Tanganyika Rift (Rukwa basin), consistent with stress inversions by *Delvaux and Barth* [2009] and recalculated focal mechanisms by *Yang and Chen* [2010].

Elastic strain accumulation profiles across segments of the rift where sufficiently dense GPS measurements exist show a fair agreement with observations (Figure 8). The agreement however depends on the location of the block boundary faults in the model, which are not very precisely determined from geological observations along a significant length of the EAR. We do reproduce the east-west velocity gradient observed at the MER in northern Ethiopia [*Kogan et al.*, 2012], but the north-south component appears inconsistent with our simplified model and could result from additional processes, perhaps magmatic [e.g., *Manighetti et al.*, 2001] or deeper seated [*Buck*, 1991, 2004]. Elastic strain accumulation appears to be a viable explanation for the reduced velocities observed at sites close to the Western branch in northern Tanganyika and northern Malawi. The fit of an elastic strain accumulation model to the GPS data in the eastern branch is less obvious, perhaps indicating that faults there are creeping and/or that magmatic processes play a significant role in extensional processes in that warmer segment of the EAR [*Calais et al.*, 2008].

6. Conclusions

We have used the most complete GPS data set to date to refine estimates of the present-day kinematics of the EAR with a model that accounts for both rigid block rotation and elastic strain accumulation on rift-bounding faults. We confirm that the kinematics of the EAR can be, to first order, described by the relative motion of two major plates, Nubia and Somalia, with three smaller microplates embedded into the plate boundary zone, Victoria, Rovuma, and Lwandle. We find that earthquake slip vectors provide information that is overall consistent with the GPS velocities and significantly helps reduce the uncertainties in plate angular velocity estimates. However, we find that 3.16 Myr average spreading rates along the Southwest Indian Ridge (SWIR) are systematically faster than GPS-derived motions across that ridge, possibly indicating the need to revise their outward displacement correction.

Our estimate of the Nubia-Somalia Euler pole appears to converge to a location similar (within uncertainties) to all recently published estimates, whether geodesy based or geology based, with, however, a slightly lower rotation rate. The location of the Victoria-Nubia Euler pole is similar to that of recent geodesy-only solutions. This is not the case for the Rovuma-Nubia pole, whose location must be outside of the Rovuma plate and south of it in order to fit earthquake slip vectors in the Urongas protorift and the Chissenga seismic zone (including the 2006, *M*7.5 purely extensional earthquake in southern Mozambique). The Lwandle angular velocity remains poorly determined but is consistent, within uncertainties, with that of *Stamps et al.* [2008].

Additional microplates or blocks, such as the Masai block in northern Tanzania [*Le Gall et al.*, 2008] or the Rukwa block in southwestern Tanzania [*Delvaux et al.*, 2012] may be required to fit future denser and more precisely determined GPS velocity fields. Deviation from the simple and uniform elastic strain accumulation model used here may emerge with dense geodetic data across rift basins and should inform on the thermal and mechanical behavior of the rift and, possibly, on the role of magmatic processes in present-day extension. However, the robust features of the kinematic model presented here can already serve as a basis for investigating the dynamics of the EAR. For instance, a mechanical explanation for the counterclockwise rotation of Victoria within a plate boundary whose kinematics is well described by clockwise rotations (of Somalia, Rovuma, and Lwandle) remains to be found.

Acknowledgments

We acknowledge and thank organizations that make their geodetic data openly available to research. We thank colleagues and students from Ardhi University, Department of Geomatics, and the University of Dar Es Salaam, Department of Geology, for the support they provided to our joint field work in Tanzania. We acknowledge the field support from the Hartebestoek Observatory, South Africa, via L. Combrinck. We thank C. DeMets for sharing GPS velocities for Antarctica ahead of publication. This work uses data services provided by the UNAVCO Facility with support from the National Science Foundation (NSF) and National Aeronautics and Space Administration (NASA) under NSF Cooperative Agreement EAR-0735156. E.C., E.S., and D.S.S. were supported by NSF award EAR-0538119 to E.C. D.S.S. was also supported by NSF graduate research fellowship EAR-2009052513. D.D. was supported by the Action 1 program of the Belgian Science Policy. We thank R. Malservisi and an anonymous reviewer for their constructive comments which significantly helped improve the original manuscript. All data used in this study are publicly available on the following public archives: AFREF [afrefdata.org], TRIGNET [www.trignet.co.za], NIGNET [server.nignet.net], UNAVCO [www.unavco.org], SIO [sopac.ucsd.edu], IGS [www.igs.org], and SEGAL [segal.ubi.pt] (provides partial data sets only). We thank all agencies and individual investigators who contribute their data through these archives. We thank the IGS and its centers for providing open GNSS data and data products to the community. All GPS data acquired by our group in East Africa via funding from the U.S. National Science Foundation (NSF) are available on the UNAVCO archive, as per NSF data policy. Ancillary information necessary to process GPS data, such as precise satellite orbits, and antenna phase center models are openly available from the IGS [www.igs.org]. Global SINEX files used here are publicly available at MIT [http://acc.igs.org/reprocess.html]. The software used to process the GPS data (GAMIT-GLOBK) is openly available at MIT [http://www-gpsg.mit.edu/~simon/gtgk]. The software used for the kinematic modeling is openly available at http://web.pdx.edu/~mccaf/www/defnode/. Earthquake slip vector directions from the CMT project are found at http://www.globalcmt.org.

References

Albaric, J., J. Déverchére, C. Petit, and B. Le Gall (2009), Crustal rheology and depth distribution of earthquakes: Insights from the central and southern East African Rift System, *Tectonophysics*, *468*(1-4), 28–41.

Altamimi, Z., X. Collilieux, and L. Métivier (2011), ITRF2008: An improved solution of the International Terrestrial Reference Frame, *J. Geod.*, *85*(8), 457–473, doi:10.1007/s00190-011-0444-4.

Altamimi, Z., L. Métivier, and X. Collilieux (2012), ITRF2008 plate motion model, *J. Geophys. Res.*, *117*, B07402, doi:10.1029/2011JB008930.

Argus, D. F., R. G. Gordon, M. B. Heflin, C. Ma, R. Eanes, P. Willis, W. R. Peltier, and S. Owen (2010), The angular velocities of the plates and the velocity of Earth's center from space geodesy, *Geophys. J. Int.*, *180*(3), 916–960, doi:10.1111/j.1365-246X.2009.04463.x.

Atwater, T., and J. D. Mudie (1973), Detailed near-bottom geophysical study of the Gorda Rise, *J. Geophys. Res.*, *78*, 8665–8686.

Biggs, J., E. Nissen, T. Craig, J. Jackson, and D. P. Robinson (2010), Breaking up the hanging wall of a rift border fault: The 2009 Karonga earthquakes, Malawi, *Geophys. Res. Lett.*, *37*, L11305, doi:10.1029/2010GL043179.

Biggs, J., F. Amelung, N. Gourmelen, T. H. Dixon, and S. W. Kim (2009), InSAR observations of 2007 Tanzania rifting episode reveal mixed fault and dyke extension in an immature continental rift, *Geophys. J. Int.*, *179*(1), 549–558, doi:10.1111/j.1365-246X.2009.04262.x.

Boyd, F. R., and J. J. Gurney (1986), Diamonds and the African lithosphere, *Science*, *232*, 472–477.

Buck, W. R. (1991), Modes of continental lithospheric extension, *J. Geophys. Res.*, *96*, 20,161–20,178.

Buck, W. R. (2004), Consequences of asthenospheric variability on continental rifting, in *Rheology and Deformation of the Lithosphere at Continental Margins*, edited by G. D. Karner et al., pp. 130, Columbia Univ. Press, New York.

Calais, E., C. J. Ebinger, C. Hartnady, and J. M. Nocquet (2006), Kinematics of the East African Rift from GPS and earthquake slip vector data, in *The Afar Volcanic Province Within the East African Rift System*, vol. 259, edited by G. Yirgu, C. J. Ebinger, and P. K. H. Maguire, pp. 9–22, Geol. Soc. Spec. Publ., London, U. K.

Calais, E., et al. (2008), Aseismic strain accommodation by slow slip and dyking in a youthful continental rift, East Africa, *Nature*, *456*(7223), 783–787.

Chesley, J. T., R. L. Rudnick, and C. T. Lee (1999), Re-Os systematics of mantle xenoliths from the East African Rift: Age, structure, and history of the Tanzanian craton, *Geochim. Cosmochim. Acta*, *63*, 1203–127.

Chu, D., and R. Gordon (1999), Evidence for motion between Nubia and Somalia along the Southwest Indian Ridge, *Nature*, *398*, 64–66.

Craig, T. J., J. A. Jackson, K. Priestly, and D. McKenzie (2011), Earthquake distribution patterns in Africa: Their relationship to variations in lithospheric and geologic structure, and their rheological implications, *Geophys. J. Int.*, *185*, 403–434.

Dawson, J. B. (1992), Neogene tectonics and volcanicity in the North Tanzania sector of the Gregory Rift Valley: Contrasts with the Kenya sector, *Tectonophysics*, *204*, 81–92.

Delvaux, D., and A. Barth (2009), African stress pattern from formal inversion of focal mechanism data. Implications for rifting dynamics, *Tectonophysics*, *482*, 105–128.

Delvaux, D., F. Kervyn, A. S. Macheyeki, and E. B. Temu (2012), Geodynamic significance of the TRM segment in the East African Rift (W-Tanzania): Active tectonics and paleostress in the Ufipa plateau and Rukwa basin, *J. Struct. Geol.*, *37*, 161–180, doi:10.1016/j.jsg.2012.01.008.

DeMets, C, R. G. Gordon, and D. F. Argus (2010), Geologically current plate motions, *Geophys. J. Int.*, *181*, 1–80, doi:10.1111/j.1365-246X.2009.04491.x.

Déprez, A., C. Doubre, F. Masson, and P. Ulrich (2013), Seismic and aseismic deformation along the East African Rift System from a reanalysis of the GPS velocity field of Africa, *Geophys. J. Int.*, *193*, 1353–1369, doi:10.1093/gji/ggt085.

Ekstrom, G., M. Nettles, and A. M. Dziewonski (2012), Physics of the Earth and planetary interiors, *Phys. Earth Planet. Inter.*, *200-201*, 1–9, doi:10.1016/j.pepi.2012.04.002.

Fenton, C. H., and J. J. Bommer (2006), The M_w7 Machaze, Mozambique, earthquake of 23 February 2006, *Seismol. Res. Lett.*, *77*, 426–439.

Furman, T., K. Kaleta, J. Bryce, and B. Hanan (2006), Tertiary mafic lavas of Turkana, Kenya: Constraints on East African plume structure and the occurrence of high-μ volcanism in Africa, *J. Petrol.*, *47*(6), 1221–1244, doi:10.1093/petrology/egl009.

George, R. M., N. Rogers, and S. Kelley (1998), Earliest magmatism in Ethiopia: Evidence for two mantle plumes in one flood basalt province, *Geology*, *26*, 923–926, doi:10.1130/0091-7613.

Green, W. V., U. Achauer, and R. P. Meyer (1991), A three-dimensional seismic image of the crust and upper mantle beneath the Kenya Rift, *Nature*, *354*, 199–203.

Grimison, N. L., and W. P. Chen (1988), Earthquakes in Davie Ridge-Madagascar region and the southern Nubian-Somalian plate boundary, *J. Geophys. Res.*, *93*, 10,439–10,450.

Gurnis, M., Mitrovica J., Ritsema J., and H. J. van Heist (2000), Constraining mantle density structure using geological evidence of surface uplift rates: The case of the African super-plume, *Geochem. Geophys. Geosyst.*, *1*, 1020, doi:10.1029/1999GC000035.

Hartnady, C. J. H. (1990), Seismicity and plate boundary evolution in southeastern Africa, *S. Afr. J. Sci.*, *93*, 473–484.

Hartnady, C. J. H., Z. Ben-Avraham, and J. Rogers (1992), Deep-ocean basins and submarine rises off the continental margin of south-eastern Africa: New geological research, *S. Afr. J. Sci.*, *88*, 534–539.

Hartnady, C. J. H. (2002), Earthquake hazard in Africa: Perspectives on the Nubia-Somalia boundary, *S. Afr. J. Sci.*, *98*, 425–428.

Hartnady, C. J. H. (2006), *Seismotectonics of Southern Mozambique, Paper Presented at 21st Colloquium on African Geology (CAG21)*, Geol. Soc. of S. Afr., Maputo, Mozambique.

Herring, T. A., R. W. King, and S. M. McClusky (2010), *Introduction to GAMIT/GLOBK Release 10.4*, Massachusetts Institute of Technology, Cambridge, Mass.

Horner-Johnson, B. C., R. G. Gordon, S. M. Cowles, and D. F. Argus (2005), The angular velocity of Nubia relative to Somalia and the location of the Nubia-Somalia-Antarctica triple junction, *Geophys. J. Int.*, *162*, 221–238, doi:10.1111/j.1365-24X.2005.02608.x.

Horner-Johnson, B. C., R. G. Gordon, and D. F. Argus (2007), Plate kinematic evidence for the existence of a distinct plate between the Nubia and Somalian plates along the Southwest Indian Ridge, *J. Geophys. Res.*, *112*, B05418, doi:10.1029/2006JB004519.

Jestin, F., P. Huchon, and J. M. Gaulier (1994), The Somali plate and the East African Riftsystem: Present-day kinematics, *Geophys. J. Int.*, *116*, 637–654.

Keir, D., I. Hamling, A. Ayele, E. Calais, C. Ebinger, and T. Wright (2009), Evidence for focused magmatic accretion at segment centers from lateral dike injections captured beneath the Red Sea Rift in Afar, *Geology*, *37*, 59–62, doi:10.1130/G25147A.1.

Kogan, L., S. Fisseha, R. Bendick, R. Reilinger, S. McClusky, R. King, and T. Solomon (2012), Lithospheric strength and strain localization in continental extension from observations of the East African Rift, *J. Geophys. Res.*, *117*, B03402, doi:10.1029/2011JB008516.

Kreemer, C., W. E. Holt, and A. J. Haines (2003), An integrated global model of present-day plate motions and plate boundary deformation, *Geophys. J. Int.*, *154*, 8–34.

Kusky, T. M., E. Toraman, and R. Raharimahefa (2007), The Great Rift Valley of Madagascar: An extension of the Africa-Somali diffusive plate boundary?, *Gondwana Res.*, *11*, 577–579.

Le Gall, B., L. Gernigon, J. Rolet, C. Ebinger, R. Gloaguen, O. Nilsen, H. Dypvik, B. Deffontaines, and A. Mruma (2004), Neogene-Recent rift propagation in Central Tanzania: Morphostructural and aeromagnetic evidence from the Kilombero area, *Geol. Soc. Am. Bull.*, *116*, 490–510.

Le Gall, B., P. Nonnotte, J. Rolet, M. Benoit, H. Guillou, M. Mousseau-Nonnotte, J. Albaric, and J. Deverchere (2008), Rift propagation at craton margin. Distribution of faulting and volcanism in the North Tanzanian Divergence (East Africa) during Neogene times, *Tectonophysics*, *448*, 1–19.

Lemaux, J., R. G. Gordon, and J.-Y. Royer (2002), The location of the Nubia-Somalia boundary along the Southwest Indian Ridge, *Geology*, *30*, 339–342.
Lithgow-Bertelloni, C., and P. G. Silveri (1998), Dynamic topography, plate driving forces and the Africa superswell, *Nature*, *395*, 269–272.
Lyons, R. P., C. A. Scholz, M. R. Buoniconti, and M. R. Martin (2011), Late Quaternary stratigraphic analysis of the Lake Malawi Rift, East Africa: An integration of drill-core and seismic resection data, *Palaeogeogr. Palaeoclimatol. Palaeoecol.*, *303*, 20–37.
Macheyeki, A. S., D. Delvaux, M. DeBatist, and A. Mruma (2008), Fault kinematics and tectonic stress in the seismically active Manyara–Dodoma Rift segment in Central Tanzania: Implications for the East African Rift, *J. Afr. Earth. Sci.*, *51*, 163–188.
Malservisi, R., U. Ugentobler, R. Wonnacott, and M. Hackl (2013), How rigid is a rigid plate? Geodetic constraint from the TrigNet CGPS network, South Africa, *Geophys. J. Int.*, *192*, 918–928, doi:10.1093/gji/ggs081.
Manighetti, I., P. Tapponnier, V. Courtillot, and Y. Gallet (2001), Strain transfer between disconnected, propagating rifts in Afar, *J. Geophys. Res.*, *106*, 13,613–13,665, doi:10.1029/2000JB900454.
McCaffrey, R. (2002), Crustal block rotations and plate coupling, in *Plate Boundary Zones, Geodynamics Series*, vol. 30, edited by S. Stein and J. Freymueller, pp. 101–122, AGU, Washington, D. C.
McCarthy, D. D., and G. Petit (2003), IERS technical note 32, Frankfurt am Main: Verlag des Bundesamts für Kartographie und Geodäsie 127 pp., paperback, ISBN 3-89888-884-3.
McDougall, I., and F. H. Brown (2009), Timing of volcanism and evolution of the northern Kenya Rift, *Geol. Mag.*, *146*(1), 34–47.
Moreau, C., J. M. Regnoult, B. Dŕuelle, and B. Robineau (1987), A new tectonic model for the Cameroon line, central Africa, *Tectonophysics*, *141*, 317–334.
Mougenot, D., M. Recq, P. Virlogeux, and C. Lepvrier (1986), Seaward extension of the East-African Rift, *Nature*, *321*, 599–603.
Njome, M. S., S. Manga, and C. E. Suh (2010), Volcanic risk perception in rural communities along the slopes of Mount Cameroon, West-central Africa, *J. Afr. Earth. Sci.*, *58*(4), 608–622, doi:10.1016/ j.jafrearsci.2010.08.007.
Nocquet, J. M., P. Willis, and S. Garcia (2006), Plate kinematics of Nubia-Somalia using a combined DORIS and GPS solution, *J. Geod.*, *80*, 591–607.
Nyblade, A. A., and S. W. Robinson (1994), The African superswell, *Geophys. Res. Lett.*, *21*(9), 765–768.
Okada, Y. (1992), Internal deformation due to shear and tensile faults in a half-space, *Bull. Seismol. Soc. Am.*, *82*, 1018–1040.
Pik, R., B. Marty, J. Carignan, and J. Lave (2003), Stability of the upper Nile drainage network (Ethiopia) deduced from (U-Th)/He thermochronometry: Implications for uplift and erosion of the Afar plume dome, *Earth Planet. Sci. Lett.*, *215*, 73–88, doi:10.1016/S0012-821X(03)00457-6.
Pik, R., B. Marty, and D. R. Hilton (2006), How many mantle plumes in Africa? The geochemical point of view, *Chem. Geol.*, *226*, 100–114, doi:10.1016/j.chemgeo.2005.09.016.
Prawirodirdjo, L., and Y. Bock (2004), Instantaneous global plate motion model from 12 years of continuous GPS observations, *J. Geophys. Res.*, *109*, B08405, doi:10.1029/2003JB002944.
Rasskazov, S. V., N. A. Logachev, A. V. Ivanov, A. A. Boven, M. N. Maslovskaya, E. V. Saranina, I. S. Brandt, and S. B. Brandt (2003), A magmatic episode in the Western Rift of East Africa (19–17 Ma), *Geol. Geofiz.*, *44*, 317–324.
Reilinger, R., et al. (2006), GPS constraints on continental deformation in the Africa-Arabia-Eurasia continental collision zone and implications for the dynamics of plate interactions, *J. Geophys. Res.*, *111*, B05411, doi:10.1029/2005JB004051.
Reznikov, M., Z. Ben-Avraham, C. Hartnady, and T. M. Niemi (2005), Structure of the Transkei Basin and Natal Valley, Southwest Indian Ocean, from seismic reflection and potential field data, *Tectonophysics*, *397*(1), 127–141.
Ritsema, J., H. J. van Heijst, and J. H. Woodhouse (1998), Complex shear wave velocity structure imaged beneath Africa and Iceland, *Science*, *286*, 1925–1928, doi:10.1126/science.286.5446.1925.
Roberts, E. M., N. J. Stevens, P. M. O'Connor, P. H. G. M. Dirks, M. D. Gottfried, W. C. Clyde, R. A. Armstrong, A. I. S. Kemp, and S. Hemming (2012), Initiation of the Western branch of the East African Rift coeval with the Eastern branch, *Nat. Geosci.*, *5*(4), 289–294, doi:10.1038/ngeo1432.
Saria, E., E. Calais, Z. Altamimi, P. Willis, and H. Farah (2013), A new velocity field for Africa from combined GPS and DORIS space geodetic solutions: Contribution to the definition of the African reference frame (AFREF), *J. Geophys. Res. Solid Earth*, *118*, 1677–1697, doi:10.1002/jgrb.50137.
Savage, J. C. (1983), A dislocation model of strain accumulation and release at a subduction zone, *J. Geophys. Res.*, *88*, 4984–4996, doi:10.1029/JB088iB06p04984.
Schmid, R., P. Steigenberger, G. Gendt, M. Ge, and M. Rothacher (2007), Generation of a consistent absolute phase-center correction model for GPS receiver and satellite antennas, *J. Geod.*, *81*, 781–798, doi:10.1007/s00190-007-0148-y.
Sella, G. F., T. H. Dixon, and A. Mao (2002), REVEL: A model for recent plate velocities from space geodesy, *J. Geophys. Res.*, *107*, ETG 11-1–ETG 11-30, doi:10.1029/2000JB00033.
Skobelev, S. F., M. Hanon, J. Klerkx, N. N. Govorova, N. V. Lukina, and V. G. Kazmin (2004), Active faults in Africa: A review, *Tectonophysics*, *380*, 131–137, doi:10.1016/j.tecto.2003.10.016.
Stamps, D., E. Calais, E. Saria, C. Hartnady, J. Nocquet, C. J. Ebinger, and R. Fernandez (2008), A kinematic model for the East African Rift, *Geophys. Res. Lett.*, L05304, doi:10.1029/2007GL032781, in press.
Stein, S., and R. G. Gordon (1984), Statistical tests of additional plate boundaries from plate motion inversions, *Earth planet. Sci. Lett.*, *69*, 401–412.
Tedesco, D., O. Vaselli, P. Papale, S. A. Carn, M. Voltaggio, G. M. Sawyer, J. Durieux, M. Kasereka, and F. Tassi (2007), January 2002 volcano-tectonic eruption of Nyiragongo volcano, Democratic Republic of Congo, *J. Geophys. Res.*, *112*, B09202, doi:10.1029/2006JB004762.
Ubangoh, R. U., B. Ateba, S. N. Ayonghe, and G. E. Ekodeck (1997), Earthquake swarms of Mt Cameroon, West Africa, *J. Afr. Earth. Sci.*, *24*(4), 413–424.
Weeraratne, D. S., D. W. Forsyth, K. M. Fischer, and A. A. Nyblade (2003), Evidence for an upper mantle plume beneath the Tanzanian craton from Rayleigh wave tomography, *J. Geophys. Res.*, *108*(B9), 2427, doi:10.1029/2002JB002273.
Wendlandt, R. F., and P. A. Morgan (1982), Lithosphere thinning associated with rifting in East Africa, *Nature*, *298*, 734–736.
Wilson, J. T. (1966), Did the Atlantic close and then re-open?, *Nature*, *211*, 676–681.
Wolfenden, E., C. Ebinger, G. Yirgu, A. Deino, and D. Ayalew (2004), Evolution of the northern Main Ethiopian Rift: Birth of a triple junction, *Earth Planet. Sci. Lett.*, *224*, 213–228.
Wonnacott, R. T. (2005), AFREF: Background and progress towards a unified reference system for Africa proceedings, FIG Working Week 2005 Cairo Egypt, 16-21 April 2005.
Wonnacott, R. T. (2006), The AFREF project: A progress report, AFREF Technical Workshop, Cape Town July 2006.

Yang, Z., and W. P. Chen (2008), Mozambique earthquake sequence of 2006: High-angle normal faulting in southern Africa, *J. Geophys. Res.*, *113*, B12303, doi:10.1029/2007JB005419.

Yang, Z., and W. P. Chen (2010), Earthquakes along the East African Rift System: A multiscale, system-wide perspective, *J. Geophys. Res.*, *115*, B12309, doi:10.1029/2009JB006779.